Whole-Body ^{18}F Dopa PET for Detection of Gastrointestinal Carcinoid Tumors[1]

Stefan Hoegerle, MD
Carsten Altehoefer, MD
Nadir Ghanem, MD
Gabriele Koehler, MD
Cornelius F. Waller, MD
Hans Scheruebl, MD
Ernst Moser, MD, PhD
Egbert Nitzsche, MD

Index terms:
Carcinoid, 70.316
Fluorine, radioactive
Gastrointestinal tract, CT, 70.12112, 70.12115
Gastrointestinal tract, MR, 70.121411, 70.121412
Gastrointestinal tract, neoplasms, 70.316
Gastrointestinal tract, PET, 70.12163
Gastrointestinal tract, SPECT, 70.12162

Published online: July 19, 2001
10.1148/radiol.2202001440
Radiology 2001; 220:373–380

Abbreviation:
FDG = 2-[fluorine 18]fluoro-2-deoxy-D-glucose

[1] From the Department of Radiology, Divisions of Nuclear Medicine (S.H., E.M., E.N.) and Diagnostic Radiology (C.A., N.G.), Department of Pathology (G.K.), and Department of Internal Medicine, Division of Hemato-oncology (C.F.W.), Albert-Ludwigs University, Hugstetterstrasse 55, 79106 Freiburg, Germany; and the Department of Gastroenterology, University Hospital Benjamin Franklin, Free University Berlin, Germany (H.S.). Received August 25, 2000; revision requested October 17; revision received December 21; accepted February 12, 2001. **Address correspondence to** S.H.

Author contributions:
Guarantors of integrity of entire study, S.H., E.N.; study concepts, S.H., E.N., E.M.; study design, S.H., E.N., C.F.W.; literature research, S.H., H.S., C.F.W.; clinical studies, S.H., E.N., C.A., N.G., G.K., C.F.W.; data acquisition, S.H., E.N., C.A., N.G., G.K.; data analysis/interpretation, S.H., E.N., C.A., N.G., C.F.W.; manuscript preparation, S.H., E.N.; manuscript definition of intellectual content, all authors; manuscript editing, S.H., E.N.; manuscript revision/review and final version approval, all authors.

PURPOSE: To evaluate fluorine 18 (^{18}F) dopa positron emission tomography (PET) in comparison with established imaging procedures in gastrointestinal carcinoid tumors.

MATERIALS AND METHODS: After evaluation of the normal distribution of ^{18}F dopa, 17 patients with histologically confirmed tumors were examined with ^{18}F dopa PET. Results of 2-[fluorine 18]fluoro-2-deoxy-D-glucose (FDG) PET, somatostatin-receptor scintigraphy, and morphologic imaging (computed tomography and/or magnetic resonance imaging) were available for all patients. Results of the procedures were evaluated by two radiologists and two nuclear medicine specialists, whose consensus based on all available histologic, imaging, and follow-up findings was used as the reference standard.

RESULTS: Ninety-two tumors were diagnosed: eight primary tumors, 47 lymph node metastases, and 37 organ metastases. ^{18}F dopa PET led to 60 true-positive findings (seven primary tumors, 41 lymph node metastases, 12 organ metastases); FDG PET, 27 (two primary tumors, 14 lymph node metastases, 11 organ metastases); somatostatin-receptor scintigraphy, 52 (four primary tumors, 27 lymph node metastases, 21 organ metastases); and morphologic imaging, 67 (two primary tumors, 29 lymph node metastases, 36 organ metastases). This resulted in the following overall sensitivities: ^{18}F dopa PET, 65% (60 of 92); FDG PET, 29% (27 of 92); somatostatin-receptor scintigraphy, 57% (52 of 92); morphologic procedures, 73% (67 of 92). Although the morphologic procedures were most sensitive for organ metastases, ^{18}F dopa PET enabled best localization of primary tumors and lymph node staging.

CONCLUSION: ^{18}F dopa PET is a promising procedure and useful supplement to morphologic methods in diagnostic imaging of gastrointestinal carcinoid tumors.

Despite the great number of existing procedures, diagnostic imaging of gastrointestinal carcinoid tumors is frequently difficult and not infrequently unsuccessful (1). The main reason is that assessment of the walls of hollow organs in the gastrointestinal tract and of lymph nodes with morphologic imaging procedures (computed tomography [CT] and magnetic resonance [MR] imaging) is limited. Therefore, diagnosis of primary tumors and lymph node staging is often unsatisfactory (2–6). On the other hand, the sensitivity of functional imaging procedures (metaiodobenzylguanidine scintigraphy or somatostatin-receptor scintigraphy) is limited because their anatomic resolution is worse (7–10). This can be compensated for only partially by the increased contrast attained with single photon emission CT (SPECT) (11). An additional limitation is the lack of tracer uptake due to deficient catecholamine stores or a lack of receptor expression (12), which may lead to false-negative findings. This is especially due to the well-known variability of biologic properties of this heterogeneous group of tumors (13).

A widespread characteristic of these tumors is the uptake and metabolization of amino acids, which resulted in the term *amine precursor uptake and decarboxylation*, or APUD, system being used to denote the diffuse neuroendocrine system (14). This property of taking up amino acids, transforming them into biogenic amines by means of decarboxylation, and storing them in vesicles was already used for imaging of neuroendocrine pancreatic tumors with carbon 11 (^{11}C) dopa (3,4-dihydroxyphenylalanine) positron

emission tomography (PET) (15,16). In addition, there is a single case report on the successful use of fluorine 18 (^{18}F) dopa PET for staging a metastasizing carcinoid tumor (17). PET offers the highest resolution among the functional methods, and the use of ^{18}F dopa, such as 2-[fluorine 18]fluoro-2-deoxy-D-glucose (FDG), enables performance of whole-body examinations in one session.

The purpose of the present study was to evaluate ^{18}F dopa whole-body PET in comparison with established imaging procedures in gastrointestinal carcinoid tumors.

MATERIALS AND METHODS

Patients

After approval by the institutional review board, 17 consecutive patients (seven women, 10 men; age range, 19–74 years; mean age, 55 years ± 16 [SD]) with histologically proved gastrointestinal carcinoid tumors were examined by means of ^{18}F dopa PET. At least one tumor had been confirmed histologically in patients with multiple metastases. All patients granted informed consent.

None of the patients presented with clinical symptoms of carcinoid syndrome. Urinary 5-hydroxyindoleacetic acid was moderately elevated in two patients. In all patients, the carcinoid tumor was found unexpectedly during surgical, endoscopic, or imaging procedures. On the basis of the unexpected finding, imaging procedures were used for staging after surgical resection of the primary tumor in seven cases: three appendiceal tumors (2.2-cm diameter, 2.0-cm diameter with solitary lymph node metastasis, and 1.7-cm diameter with infiltration of the mesoappendix), two ileal tumors, one colonic tumor within an intestinal polyp, and one rectal tumor. In the remaining 10 patients, no previous surgery had been performed. After staging in all patients, surgery was performed in six; no surgery was performed in the other 11 patients.

In all patients, results of morphologic imaging (CT and/or MR imaging), somatostatin-receptor scintigraphy, and FDG PET were available as part of clinical routine staging. All of the imaging procedures were performed within a maximum of 6 weeks after the tumor was found.

Histologic and Immunohistochemical Findings

Carcinoid tumors were diagnosed on the basis of the histologic findings and additional immunohistochemical tests in which the expression of neuroendocrine tumor markers such as synaptophysin, neuron-specific enolase, or chromogranin was examined. According to recent classifications, all cases were malignant carcinoid tumors that were subdivided into categories of high, moderate, or low differentiation (13,18). All preparations were tested by using standard immunohistochemical procedures for serotonin expression. Histologic and immunohistochemical examinations were performed by one pathologist (G.K.) blinded to the imaging findings.

FDG and ^{18}F Dopa PET

All patients fasted for 12 hours prior to the start of the examination to provide optimal conditions for uptake of the radiopharmaceuticals. Blood glucose levels were controlled in all patients for the FDG PET; none was greater than normal (110 mg/dL [6.1 mmol/L]). For FDG PET, 360 MBq ± 30 of FDG was injected intravenously; for ^{18}F dopa PET, 200 MBq ± 30 of ^{18}F dopa was injected intravenously. Both radiopharmaceuticals were produced by using standard procedures (19,20). The uptake time was 90 minutes for FDG to attain optimization of the tumor-to-background ratio. For ^{18}F dopa, the uptake time was 60–90 minutes, which is analogous to the uptake time for brain examinations (21). Data were acquired with a two-dimensional ring scanner (Ecat Exact; Siemens/CTI, Knoxville, Tenn) with a rod source by using postinjection segmented attenuation correction. Eight to 10 bed positions with an 11-cm transverse field of view were measured (2 minutes transmission and 8 minutes emission per position). Images were reconstructed by means of an iterative procedure with ordered subsets (ordered subset-expectation maximization, or OSEM, two iterations, eight subsets) (22), no pre- or postfiltering was used, and final reconstruction resolution of the images was 6 mm.

Comparison with Control Group

The study group was compared with a control group to determine normal distribution of ^{18}F dopa in the body. The control group consisted of five consecutive patients (three men, two women; age range, 42–73 years; mean age, 57 years) in whom an examination with ^{18}F dopa was clinically indicated for Parkinson disease. None of the control subjects had malignant disease.

Somatostatin-Receptor Scintigraphy

After intravenous injection of 170 MBq ± 25 of indium 111 pentetreotide (OctreoScan; Mallinckrodt, Petten, the Netherlands), planar scintigrams were obtained with a large-field-of-view gamma camera (Bodyscan; Siemens, Erlangen, Germany) and a medium-energy collimator. Four hours and 24 hours after injection, ventral and dorsal whole-body images were acquired, and target images of the abdomen and thorax were also obtained. The SPECT examination of the thorax and abdomen was performed 24 hours after injection by using a triple-headed camera (Prism XP 3000; Picker Marconi, Cleveland, Ohio) with the following parameters: 128 × 128 matrix, 120 projections in 3° angle increments, and 40-second acquisition time per projection. Images were reconstructed by using filtered back-projection: no prefiltering, reconstruction with ramp filter, and postprocessing with a low-pass filter with a cutoff frequency corresponding to a 5% noise level, order of five.

Interpretation of the PET Images and Somatostatin-Receptor Scintigrams

The reconstructed images were assessed by two nuclear medicine specialists (S.H., E.N.) on a standard computer monitor (Sun Microsystems, San Diego, Calif) at all three levels (transverse, coronal, and sagittal views) by using an inverse gray scale. Somatostatin-receptor scintigrams and FDG and ^{18}F dopa PET scans in each patient were interpreted at different times, with the readers blinded to the results of the other studies. Images were interpreted by means of consensus of the two nuclear medicine specialists; there were no discrepancies. Any focal tracer accumulation exceeding normal regional tracer uptake was rated as a pathologic finding—a tumor. These pathologic findings were classified as primary tumors (lesion within the intestine), lymph node metastases (tracer accumulations in regional and distant lymph nodes), and organ metastases (pathologic uptake in parenchymatous organs such as the liver or lungs). Intestinal uptake that was linearly and nonfocally limited was rated as a nonspecific nonpathologic finding.

Morphologic Imaging

Morphologic imaging was performed according to standard protocols. Abdominal CT and/or MR images were available for all patients; additional thoracic CT examinations were performed in all patients with proved abdominal tumors to detect potential tumors in the thorax.

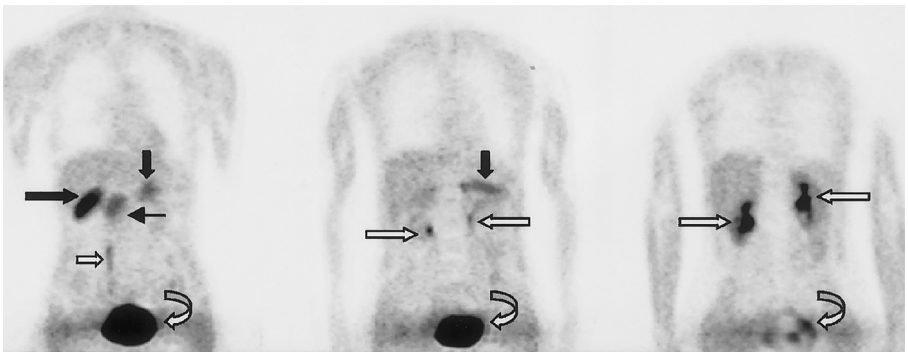

Figure 1. Possible Parkinson disease in a 53-year-old woman. Representative coronal ^{18}F dopa PET images (sequence from left to right is ventral to dorsal) show normal distribution of the radiopharmaceutical in the trunk. Physiologically, the gallbladder (long thick black arrow), parts of the pancreas (short thick black arrows), duodenum (thin black arrow) and renal collecting system (long white arrows), right-side ureter (short white arrow), and urinary bladder (curved arrows) are depicted.

Since the decision whether to use CT and/or MR imaging was made within the clinical routine independent of this study, it can be considered randomized: There were nine patients with abdominal CT scans, six patients with abdominal MR images, and two with both.

CT examinations were performed with two scanners (Somatom Plus 4 or Somatom Plus S; Siemens). Abdominal helical CT was performed with 70–120 mL of intravenously administered iopromide (Ultravist 300; Schering, Berlin, Germany) and included the portal venous phase. In addition, the gastrointestinal tract was imaged after oral administration of diluted diatrizoate meglumine (Gastrografin; Schering). Collimation was set to 8 or 10 mm at a table feed of 12 or 15 mm; the reconstruction interval was 8 or 10 mm. For thoracic helical CT, 70–100 mL of iopromide was administered intravenously, and the following scanning parameters were used: collimation of 8 or 10 mm, table feed of 12 or 15 mm, and reconstruction interval of 8 or 10 mm.

Static abdominal MR images were acquired with 1.5-T imagers (Magnetom Vision or Magnetom Symphony; Siemens) by using a body coil or body phased-array coil for signal reception. The upper abdomen was imaged during a single breath hold by using nonenhanced T2-weighted turbo spin-echo sequences (2,800–3,200/120–138 [repetition time msec/echo time msec]), nonenhanced T1-weighted gradient-echo sequences (fast low angle shot, 87–148/4.0–4.8, 70° flip angle), and gadolinium-enhanced T1-weighted gradient-echo sequences after spectral fat saturation (104–168/4.0–4.8). The standard dose of 0.1 mmol of gadopentetate dimeglumine (Magnevist; Schering) per kilogram of body weight was administered intravenously. Pelvic MR imaging with a phased-array coil and abdominal MR imaging with a body coil were performed without breath hold. T2-weighted turbo spin-echo sequences (4,700/120–138) and nonenhanced and gadolinium-enhanced T1-weighted spin-echo sequences (500–750/12–15) were used. The section thickness was 6–8 mm for all sequences.

Interpretation of Morphologic Images

Images were interpreted by two radiologists (C.A., N.G.) blinded to the results of the scintigraphic and PET examinations. If CT and MR imaging had been performed in the same patient, both examinations were assessed at the same time. Images were interpreted by means of consensus of the two radiologists. Every contrast medium–enhancing tumor within the walls of the hollow organs of the gastrointestinal tract was rated as a primary tumor. Lesions within parenchymatous organs were rated as organ metastases if they were not clearly identified as benign lesions (eg, cystic lesions or hemangiomas) according to standard criteria (attenuation or signal intensity and enhancement pattern after administration of contrast medium). Lymph nodes were staged morphologically according to the standard criterion of nodal diameter. Lymph nodes with a diameter as large as 1 cm were rated as tumor free, and lymph nodes with a diameter of more than 1 cm in the longest axis were rated as lymph node metastases (5,6,23). No other lymph node criteria were assessed.

Data Evaluation

Since not all lesions could be histologically proved and the different imaging modalities frequently showed discrepancies, the results of the individual imaging procedures were evaluated as follows. The results of the individual procedures were interpreted by the two radiologists and the two nuclear medicine specialists without knowledge of clinical data or other findings, as described earlier. For further data evaluation, a committee consisting of the two radiologists and the two nuclear medicine specialists achieved a consensual diagnosis regarding the presence of tumor and the number and localization of tumors in each patient.

This consensus, serving as the reference standard against which the results of the individual procedures were measured, was based on histologic findings in surgical specimens in 31 lesions or the results of all of the imaging procedures, with inclusion of serial follow-up morphologic imaging, in 61 lesions. On the basis of these data, no discrepancies between radiologists and nuclear medicine specialists were observed. All lesions detected solely by means of ^{18}F dopa PET were accepted for the reference standard only on condition that the specific lesion was histologically verified or that a correlate in morphologic imaging was present initially or disclosed at follow-up examinations (eg, a lymph node initially not fulfilling the morphologic criterion of malignancy [<1 cm] but showing ^{18}F dopa accumulation and increasing size at follow-up examinations). This consensus procedure resulted in a set of data for each patient with respect to primary tumor, lymph node status, and organ metastases. Sensitivity and specificity of the individual procedures were calculated from these data.

RESULTS

Control Group

With the exception of intestinal uptake, all of the persons in the control group showed a uniform distribution pattern of ^{18}F dopa in the body (Fig 1). Although no tracer accumulations were observed in the neck and thorax, the bile ducts, especially the gallbladder, and the urogenital system (renal pelvis, ureter, and urinary bladder) showed distinct tracer uptake in all patients. In the intestinal tract, slight contrasting of the duodenum and parts of the pancreas was observed in all subjects. In three patients, there were linear nonfocal limited accu-

TABLE 1
Number of Tumors Diagnosed with the Different Imaging Procedures

Patient No.	Previous Surgery	Subsequent Surgery	Histologic Differentiation	Immunohistochemical Finding of Serotonin	F^{18} Dopa PET	FDG PET	SRS*	CT and/or MR Imaging	Consensus
1	No	No	High	Positive	9†	0	3	8	9†
2	Yes (appendix)	No	Moderate	Positive	0	0	0	0	0
3	No	Yes	High	Positive	15†	5	7	7	15†
4	Yes (rectum)	No	Moderate	Negative	1†	2†	5†	6†	6†
5	Yes (colon polyp)	Yes	High	Positive	2†	0	1†	0	1
6	Yes (ileum)	No	Moderate	Positive	2	2	4	5	5
7	No	Yes	High	Positive	1	0	2†	1	2†
8	No	No	Moderate	Negative	1	1	8	8	8
9	Yes (appendix)	No	Moderate	Positive	0	0	0	0	0
10	No	No	Adenocarcinoma	Negative	0	28†	0	27†	28†
11	No	No	High	Negative	0	1	3	4	4
12	No	Yes	Moderate	Positive	4†	2†	3†	2	4†
13	Yes (ileum)	Yes	High	Positive	1†	0	0	1	1†
14	No	No	High	Positive	23†	7	13†	16†	24†
15	No	Yes	Moderate	Positive	2†	1	1	1	2†
16	Yes (appendix)	No	Moderate	Positive	0	0	0	0	0
17	No	No	Moderate	Negative	0	6	3	11	11

* SRS = somatostatin-receptor scintigraphy.
† Primary tumor, residual tumor, or local recurrence.

TABLE 2
Results of the Imaging Procedures

	F^{18} Dopa PET				FDG PET				SRS*				CT and/or MR Imaging				CT and/or MR Imaging with F^{18} Dopa PET				
Lesion	TP	TN	FP	FN	TP	TN	FP	FN	TP	TN	FP	FN	TP	TN	FP	FN	TP	TN	FP	FN	Consensus
Primary tumor	7	7	1	1	2	8	0	6	4	7	1	4	2	8	0	6	7	7	1	1	8
Lymph node metastases	41	8	0	6	14	8	0	33	27	8	0	20	29	8	0	18	47	8	0	0	47
Organ metastases	12	8	0	25	11	8	0	26	21	8	0	16	36	8	2	1	37	8	2	0	37
Overall	60	25	1	32	27	24	0	65	52	23	1	40	67	24	2	25	91	23	3	0	92

Note.—Data are the number of lesions and exclude patient 10, in whom the original histologic findings were later revised. FN = false-negative finding, FP = false-positive finding, TN = true-negative finding, TP = true-positive finding.
* SRS = somatostatin-receptor scintigraphy.

TABLE 3
Calculated Sensitivities of the Imaging Procedures

Lesion	F^{18} Dopa PET	FDG PET	SRS*	CT and/or MR Imaging	CT and/or MR Imaging with F^{18} Dopa PET
Primary tumor (n = 8)	88 (7)	25 (2)	50 (4)	25 (2)	88 (7)
Lymph node metastases (n = 47)	87 (41)	30 (14)	57 (27)	62 (29)	100 (47)
Organ metastases (n = 37)	32 (12)	30 (11)	57 (21)	97 (36)	100 (37)
Overall (n = 92)	65 (60)	29 (27)	57 (52)	73 (67)	99 (91)

Note.—Data are percentages. Numbers in parentheses are the number of lesions found with each modality.
* SRS = somatostatin-receptor scintigraphy.

mulations in the intestine. These were apparently nonpathologic normal variants, most likely bile within the intestine.

Study Group

The results of the various imaging procedures for each patient are presented in Table 1. Patient 10 could not be included in the final assessment, since the original histologic findings were later revised. This patient had been referred with histologically confirmed multiple hepatic metastases of a gastrointestinal carcinoid tumor with unknown primary localization. Both somatostatin-receptor scintigraphy and ^{18}F dopa PET showed completely normal findings, whereas FDG PET showed pronounced metastatic hepatic disease with multiple other tumors in the lungs, mediastinum, and pelvic skeleton. Because of this pattern of findings, which is unusual for a carcinoid tumor, the histologic findings were reviewed a second time; the revised finding was a pulmonary adenocarci-

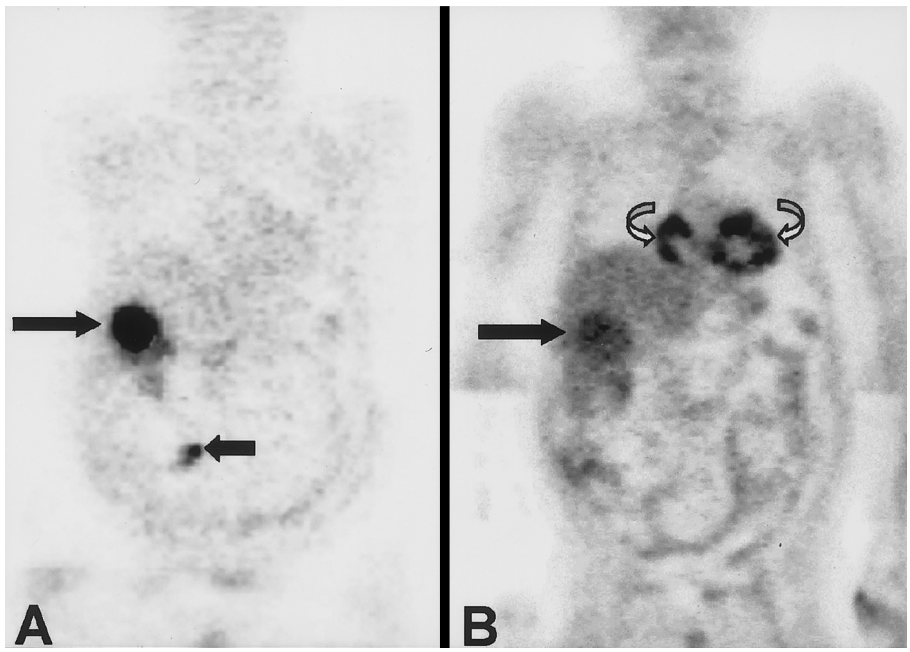

Figure 2. Known hepatic metastasis of a neuroendocrine tumor in a 62-year-old man. Coronal ^{18}F dopa PET image *(A)* clearly shows the small primary tumor (short arrow) in a loop of the ileum, in addition to the known hepatic metastasis (long arrow). Coronal FDG PET image *(B)* does not depict the primary tumor, and even the hepatic metastasis (straight arrow) shows only a slightly elevated glucose metabolism. Despite a 12-hour fast, pronounced FDG accumulation is found as a normal variant in the myocardium of the right and left ventricles (curved arrows).

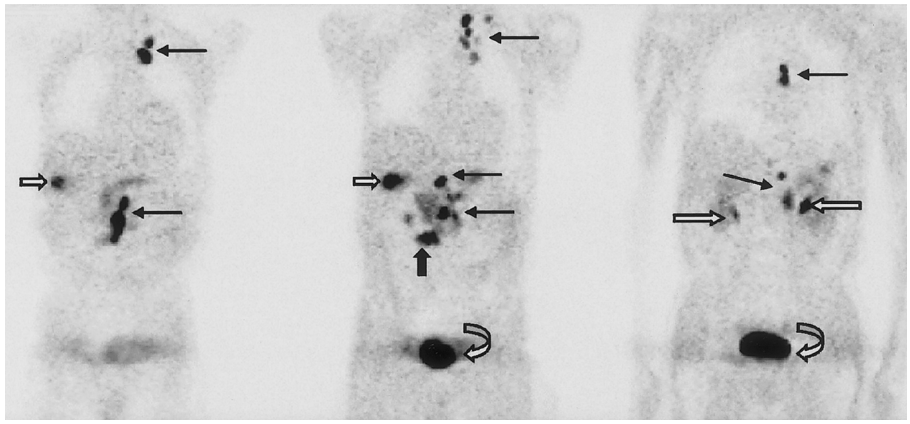

Figure 3. Lymphogenic metastasizing ileal tumor in a 64-year-old man. Coronal ^{18}F dopa PET images (sequence from left to right is ventral to dorsal) show the primary tumor (thick black arrow) and multiple lymph node metastases (thin black arrows). In addition, there are physiologic ^{18}F dopa accumulations in the gallbladder (short straight white arrows), renal collecting system (long straight white arrows), and urinary bladder (curved arrows).

noma with only slight neuroendocrine subpopulation.

The results of the individual imaging procedures compared with the reference standard are listed in Table 2; data refer to the remaining 16 patients. The greatest number of true-positive findings was obtained with morphologic imaging, followed by ^{18}F dopa PET, somatostatin-receptor scintigraphy, and FDG PET.

After subdivision of the results into the categories of primary tumors, lymph node metastases, and organ metastases, the morphologic procedures were most sensitive in the detection of organ metastases, whereas diagnosis of primary tumor and lymph node staging were considerably less reliable. The best results with respect to these latter two evaluation categories were obtained with ^{18}F dopa PET. By using a combination of morphologic imaging and ^{18}F dopa PET, seven of eight primary tumors, all lymph node metastases, and all organ metastases were correctly identified.

Table 3 shows the sensitivities of the individual procedures calculated on the basis of the applied reference standard, which cannot yet be considered optimal (see Discussion). Since all of the procedures led to only isolated false-positive results that were confirmed with histologic or follow-up findings, specificity was greater than 90% for all of the imaging methods.

In 38% (six of 16) of the patients, ^{18}F dopa PET produced additional information that was obtained with none of the other imaging procedures. By using ^{18}F dopa PET, it was possible in three of these patients to localize the previously unknown primary tumors (Fig 2) that were confirmed by means of histologic examination in two patients and follow-up in one patient. In one patient, ^{18}F dopa PET enabled proof of a local tumor recurrence that was histologically confirmed. In four patients, previously unknown lymph node or organ metastases were diagnosed. Of the 18 lymph node metastases detected solely by means of ^{18}F dopa PET, seven were confirmed histologically, and the remaining 11 nodes initially showed a morphologic correlate (lymph nodes $<$1 cm) or were confirmed at follow-up examination. The one organ metastasis was also confirmed by means of follow-up morphologic imaging.

In 31% (five of 16) of the patients, the results of ^{18}F dopa PET resulted in modification or even complete change in therapeutic strategy. In three of these patients, the results led to surgical intervention with the aim of potentially curative outcome. In two asymptomatic patients, the extent of metastasis became clear (Fig 3), so surgical reduction of the tumor was not performed. In one patient, however, palliative surgery was performed later owing to symptoms of intestinal stenosis.

At all of the functional imaging procedures, considerable variability of tracer uptake was observed in the individual tumors (Table 1, Figs 4, 5). Comparison of histologic and immunohistochemical findings showed that 84% (27 of 32) of the total number of false-negative ^{18}F dopa PET findings were observed in patients with non–serotonin-expressing tumors, whereas only 16% (five of 32) of false-negative findings were in patients with serotonin-expressing tumors. In all seven of the patients in whom ^{18}F dopa PET showed all tumors in agreement with

the reference standard, the tumors were highly (n = 5) or moderately (n = 2) differentiated serotonin-expressing tumors.

DISCUSSION

The results of this study help confirm that ^{18}F dopa PET enables diagnostic imaging of gastrointestinal carcinoid tumors. Initial experience shows that the results with respect to primary tumor localization and lymph node staging are better than those of the established imaging procedures; serotonin-expressing tumors are apparently especially well depicted with ^{18}F dopa PET. Moreover, the data demonstrate that carcinoid tumors require extensive diagnostic testing, since adequate diagnostic certainty is not attained with any single imaging procedure. The best possible results were obtained with a combination of ^{18}F dopa PET and morphologic imaging with CT and/or MR imaging, since these procedures complement one another to a nearly optimal degree.

Although morphologic imaging procedures showed the greatest sensitivity with respect to the total number of tumors, it was again confirmed that localization of primary tumor and lymph node staging are not satisfactory. The reasons for this may lie in the fact that primary tumors are often small and situated in the walls of hollow organs (1,13). The weakness of morphologic lymph node staging is the known lack of reliable criteria, since assessment can be made only on the basis of size (5,6,23). Owing to this uncertainty, the size limits vary slightly, and some examiners use the longest lymph node axis, whereas others use the shortest axis.

Because of the disadvantages cited, several functional imaging procedures such as metaiodobenzylguanidine scintigraphy and somatostatin-receptor scintigraphy have been developed (7,8), and somatostatin-receptor scintigraphy is currently the nuclear medical procedure of choice (10). Sensitivities of 44%–84% (cumulative sensitivity, 70%) have been reported for metaiodobenzylguanidine scintigraphy, and sensitivities of 71%–100% (cumulative sensitivity, 86%) have been reported for somatostatin-receptor scintigraphy (10). On the basis of these results alone, the procedures cannot be considered optimal.

Since small tumors (<1 cm) were frequently not imaged at somatostatin-receptor scintigraphy in the present study and even larger tumors showed no somatostatin-receptor expression in many cases, the results for somatostatin-receptor scintigraphy in this study (overall sensitivity, 57%) were even lower than those in the literature (9,10). This is probably because the sensitivity of somatostatin-receptor scintigraphy was frequently determined by means of comparison with morphologic imaging, which is limited, as discussed earlier. If only the estab-

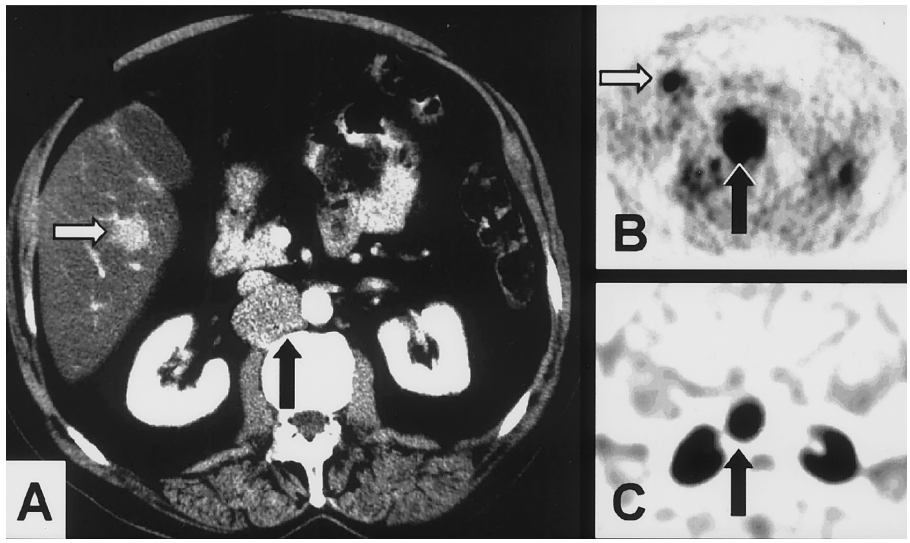

Figure 4. Ileal tumor with multiple metastases in a 61-year-old man. Whereas transverse CT *(A)* and transverse ^{18}F dopa PET *(B)* images both show a retroperitoneal lymph node metastasis (black arrows) and a hepatic metastasis (white arrows), the corresponding transverse somatostatin-receptor image obtained by means of SPECT *(C)* depicts only the lymph node metastasis (arrow). The hepatic metastasis apparently shows no receptor expression.

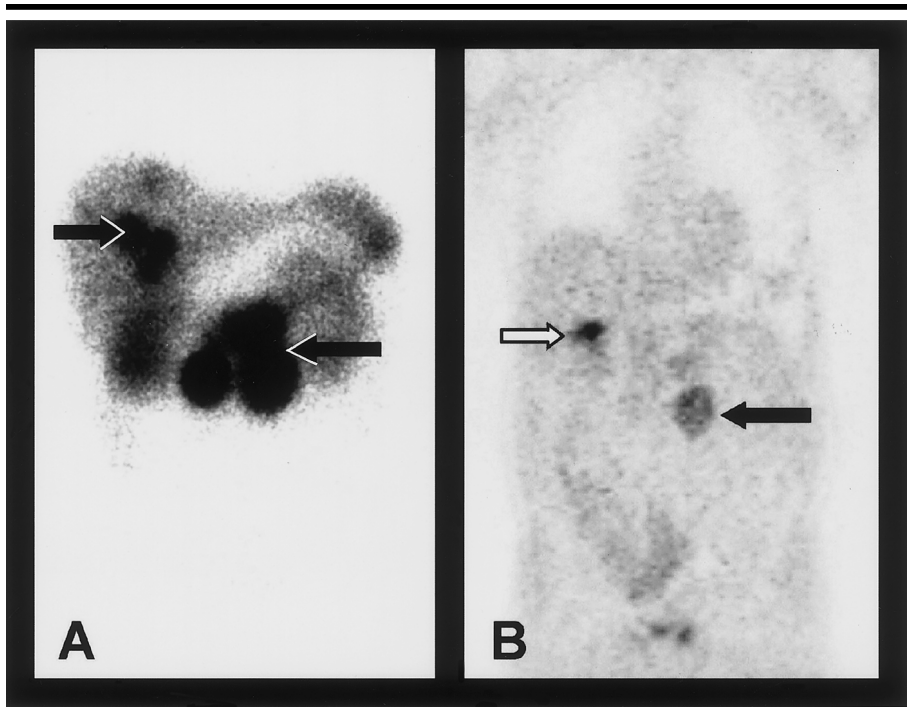

Figure 5. Metastases of an unknown primary tumor in a 59-year-old man. Coronal somatostatin-receptor scintigram *(A)* and CT scan (not shown) both revealed all known tumors—multiple serotonin-negative lymph node metastases (long black arrow) and multiple hepatic metastases (short black arrow)—whereas the coronal ^{18}F dopa PET image *(B)* showed only moderate ^{18}F dopa accumulation in one of the lymph node metastases (black arrow) and normal uptake in the gallbladder (white arrow).

lished imaging procedures had been compared in the present study, all lesions detected solely by means of ^{18}F dopa PET would not have been detected (n = 22). This would have resulted in a sensitivity of 74% (52 of 70) for somatostatin-receptor scintigraphy, which is within the range of previously published data (10).

The main advantage of lymph node staging with ^{18}F dopa PET is that, particularly in serotonin-expressing carcinoid tumors (patients 1, 3, and 14 in Table 1), the benign or malignant nature of even small lymph nodes (<1 cm) can be classified. These nodes are hardly detectable at planar or SPECT imaging and are not unequivocally assessable at morphologic imaging. This sensitive detection of small tumors leads to an improvement of the reference standard, which is identical to the verified ^{18}F dopa PET findings in some patients. Despite this advanced reference standard, criticism of several points is appropriate. The sensitivity of 100% (47 of 47) for lymph node staging in the combination of ^{18}F dopa PET and morphologic imaging is not a realistic value, and it is only because all lymph node metastases negative at ^{18}F dopa PET had a diameter considerably greater than 1 cm. However, it is plausible or even probable that individual lymph node metastases showed no ^{18}F dopa accumulation and also were not enlarged. Since the other functional methods also did not show additional lymph node metastases, and surgical exploration with histologic analysis was not possible in a majority of cases, such findings would not have been detected.

Little experience has been gained thus far with respect to PET of neuroendocrine tumors. To date, FDG, ^{11}C hydroxytryptophan, and ^{11}C dopa have been used as radiopharmaceuticals (15,24,25).

Although ^{18}F dopa has been used thus far almost exclusively for brain examinations (21,26), it also enables whole-body examinations for neuroendocrine tumors such as carcinoid tumors (17). However, similar to ^{11}C dopa uptake (15), there is a considerable variability in tracer uptake. This variability can be explained with the heterogeneous nature of neuroendocrine gastrointestinal tumors, which present considerable differences in biologic, histologic, and clinical characteristics. The variation ranges from classic highly differentiated carcinoid tumors to poorly differentiated neuroendocrine carcinomas (small cell carcinomas) (13). Because of this heterogeneity, there are various classifications that differ in a number of criteria (18). Among these criteria are the silver affinity, histologic growth pattern, localization of the primary tumor, tumor diameter, metastasis, and hormone production. In the current study, the tumors were classified only according to biologic behavior (benign or malignant), degree of differentiation, and serotonin expression.

Comparison with the histologic and immunohistochemical findings shows that serotonin-expressing tumors especially take up ^{18}F dopa. Immunohistochemically, general neuroendocrine tumor markers such as the neuron-specific enolase, synaptophysin, and chromogranin, and the cell-specific markers such as peptide hormones and biogenic amines (dopamine, serotonin), can be differentiated (1,27). Because ^{11}C dopa is decarboxylated in pancreatic tumors (16), the uptake mechanism is attributed to the long-known fact that neuroendocrine tumors are capable of taking up amino acids, transforming them by means of decarboxylation to biogenic amines, and then storing them in vesicles (14). This gives rise to the hypothesis that only amine-producing tumors can be imaged with ^{18}F dopa PET. However, this hypothesis has to be proved in further studies.

In a majority of cases, the tumors are of high and moderate differentiation, so they are difficult to image with FDG PET because of slow growth and largely normal glucose metabolism (24). This phenomenon was demonstrated especially in lymphomas and in differentiated thyroid carcinomas, which lose their capacity to store radioiodine with increasing malignancy and undifferentiation, whereas glycolysis and thus FDG storage increase at the same time (28,29). The poor results of FDG PET in the present study can be explained with this hypothesis.

Potential limitations of ^{18}F dopa PET are the substantial physiologic uptake in the duodenum and pancreas, which might mask tumors in these sites, and the unspecific accumulations within the intestine, which might lead to false-positive results.

Despite the promising results of ^{18}F dopa PET, no basic recommendations to replace the established somatostatin-receptor scintigraphy with ^{18}F dopa PET can be made. Rather, somatostatin-receptor scintigraphy will retain its validity, since apparently some carcinoid tumors manifest with somatostatin-receptor expression but do not take up ^{18}F dopa. Moreover, somatostatin-receptor expression is frequently tested if somatostatin analogues, for which both nonradioactive substances and substances emitting β radiation are available, are used palliatively (30,31).

Since both ^{18}F dopa PET and somatostatin-receptor scintigraphy are expensive procedures and cost is increasingly important, routine use of both procedures in combination with morphologic imaging procedures cannot be realized in all cases. However, additional use of ^{18}F dopa PET appears reasonable as part of staging when there is an immunohistochemical finding from a tumor with serotonin expression. In the current study, the results of ^{18}F dopa PET had an important influence on further therapy in nearly one-third of the patients. A savings potential arises thanks to improved coordination of therapeutic measures with the individual tumor spread. On the one hand, unnecessary surgery, which is stressful for the patient, is avoided; on the other hand, the localization of the primary tumor can support potentially curative surgical therapy when there is little or no metastasis. This is especially important in the case of carcinoid tumors, since complete resection is the only potentially curative therapeutic approach (1,32) and should thus lead to a reduction in cost later.

Basic limitations of this study were that the number of patients was small and that the diagnostic imaging procedures were performed only after the initial surgery in some patients. This situation was unavoidable because of unexpected intraoperative findings. Moreover, only one-third of the lesions could be verified histologically, which would have been the only real reference standard. This limitation results in a certain unreliability of all statistical values calculated in this study. However, this weakness was unavoidable because in a majority of patients, postoperative staging either brought no evidence of additional tumors or surprisingly numerous tumors were diagnosed, which made surgical therapy with histologic assessment impossible.

In conclusion, ^{18}F dopa PET is a promising imaging procedure and useful supplement to morphologic imaging methods, since it improves localization of primary tumors and lymph node staging of gastrointestinal carcinoid tumors.

References

1. Vinik AI, McLeod MK, Fig LM, Shapiro B, Lloyd RV, Cho K. Clinical features, diagnosis, and localization of carcinoid tumors and their management. Gastroenterol Clin North Am 1989; 18:865–896.
2. Picus D, Glazer HS, Levitt RG, Husband

JE. Computed tomography of abdominal carcinoid tumors. AJR Am J Roentgenol 1984; 143:581–584.
3. Laurent F, Raynaud M, Biset JM, Boisserie-Lacroix M, Grelet P, Drouillard J. Diagnosis and categorization of small bowel neoplasms: role of computed tomography. Gastrointest Radiol 1991; 16:115–119.
4. Sugimoto E, Lorelius LE, Eriksson B, Oberg K. Midgut carcinoid tumours: CT appearance. Acta Radiol 1995; 36:367–371.
5. Bollen EC, Goei R, van't Hof-Grootenboer BE, Versteege CW, Engelshove HA, Lamers RJ. Interobserver variability and accuracy of computed tomographic assessment of nodal status in lung cancer. Ann Thorac Surg 1994; 58:158–162.
6. Gdeedo A, Van Schil P, Corthouts B, Van Mieghem F, Van Meerbeck, Van Marck E. Comparison of imaging TNM [(i)TNM] and pathological TNM [pTNM] in staging of bronchogenic carcinoma. Eur J Cardiothorac Surg 1997; 12:224–227.
7. Feldman JM, Blinder RA, Lucas KJ, Coleman RE. Iodine 131 metaiodobenzylguanidine scintigraphy of carcinoid tumors. J Nucl Med 1986; 27:1691–1696.
8. Krenning EP, Bakker WH, Breeman WAP, et al. Localisation of endocrine-related tumours with radioiodinated analogue of somatostatin. Lancet 1989; 1:242–244.
9. Kwekkeboom DJ, Krenning EP, Bakker WH, Oei HY, Kooij PPM, Lamberts SWJ. Somatostatin analogue scintigraphy in carcinoid tumours. Eur J Nucl Med 1993; 20:283–292.
10. Hoefnagel CA. Metaiodobenzylguanidine and somatostatin in oncology: role in the management of neural crest tumours. Eur J Nucl Med 1994; 21:561–581.
11. Schillaci O, Scopinato F, Angeletti S, et al. SPECT improves accuracy of somatostatin receptor scintigraphy in abdominal carcinoid tumors. J Nucl Med 1996; 37: 1452–1456.
12. Reubi JC, Kvols LK, Waser B, et al. Detection of somatostatin receptors in surgical and percutaneous needle biopsy samples of carcinoids and islet cell carcinomas. Cancer Res 1990; 50:569–577.
13. Kloeppel G, Heitz PU, Capella C, Solcia E. Pathology and nomenclature of human gastrointestinal neuroendocrine (carcinoid) tumors and related lesions. World J Surg 1996; 20:132–141.
14. Pearse AGE. The cytochemistry and ultrastructure of polypeptide hormone producing cells of the APUD series and the embryologic, physiologic and pathologic implications of the concept. J Histochem Cytochem 1969; 17:303–313.
15. Ahlström H, Eriksson B, Bergström M, Bjurling P, Langström B, Öberg K. Pancreatic neuroendocrine tumors: diagnosis with PET. Radiology 1995; 195:333–337.
16. Bergström M, Eriksson B, Öberg K, et al. In vivo demonstration of enzyme activity in endocrine pancreatic tumors: decarboxylation of carbon-11-DOPA to carbon-11-dopamine. J Nucl Med 1996; 37: 32–37.
17. Hoegerle S, Schneider B, Kraft A, Moser E, Nitzsche EU. Imaging of a metastatic gastrointestinal carcinoid by F-18-DOPA positron emission tomography. Nuklearmedizin 1999; 38:127–130.
18. Capella C, Heitz PU, Hoefler H, Solcia E, Kloeppel G. Revised classification of neuroendocrine tumors of the lung, pancreas and gut. Digestion 1994; 55(suppl 3):11–23.
19. Luxen A, Perlmutter M, Bida GT, et al. Remote, semiautomated production of 6-[F-18]fluoro-L-dopa for human studies with PET. J Appl Radiat Isot 1990; 41:275–281.
20. Mulholland GK. Simple rapid hydrolysis of acetyl protecting groups in FDG synthesis using cation exchange resins. Nucl Med Biol 1995; 22:19–23.
21. Huang SC, Yu DC, Bario JR, et al. Kinetics and modeling of L-6-[18F]fluoro-dopa in human positron emission tomographic studies. J Cereb Blood Flow Metab 1991; 11:898–913.
22. Hudson HM, Larkin RS. Accelerated image reconstruction using ordered subsets of projection data. IEEE Trans Med Imaging 1994; 13:601–609.
23. Stomper P. Cancer imaging manual. Philadelphia, Pa: Lippincott, 1993; 51–61.
24. Adams S, Baum R, Rink T, Schumm-Dräger PM, Usadel KH, Hör G. Limited value of fluorine-18 fluorodeoxyglucose positron emission tomography for the imaging of neuroendocrine tumours. Eur J Nucl Med 1998; 25:79–83.
25. Eriksson B, Bergstrom M, Lilja A, Ahlstrom H, Langstrom B, Oberg K. Positron emission tomography (PET) in neuroendocrine gastrointestinal tumors. Acta Oncol 1993; 2:189–196.
26. Martin WRW, Palmer MR, Patlak CS, Calne DB. Nigrostriatal function in humans studied with positron emission tomography. Ann Neurol 1989; 26:535–542.
27. Memon MA, Nelson H. Gastrointestinal carcinoid tumors: current management strategies. Dis Colon Rectum 1997; 40: 1101–1118.
28. Okada J, Oonishi H, Yoshikawa K, et al. FDG-PET for predicting the prognosis of malignant lymphoma. Ann Nucl Med 1994; 8:187–191.
29. Feine U, Lietzenmayer R, Hanke JP, Held J, Wohrle H, Mueller-Schauenburg W. Fluorine-18-FDG and iodine-131-iodide uptake in thyroid cancer. J Nucl Med 1996; 37:1468–1472.
30. Kvols LK, Moertel CG, O'Connell MJ, Schutt AJ, Rubin J, Hahn RG. Treatment of the malignant carcinoid syndrome: evaluation of a long-acting somatostatin analogue. N Engl J Med 1986; 315:663–666.
31. Otte A, Herrmann R, Heppeler A, et al. Yttrium-90 DOTATOC: first clinical results. Eur J Nucl Med 1999; 26:1439–1447.
32. Stinner B, Kisker O, Zielke A, Rothmund M. Surgical management for carcinoid tumors of small bowel, appendix, colon and rectum. World J Surg 1996; 20:183–188.